Technische Universität Berlin
Institut für Mathematik

Optimization of a thermal coupled flow problem part I: Algorithms and numerical results

Günter Bärwolff   Michael Hinze

Optimization of a thermally coupled flow problem part I: Algorithms and numerical results

Günter Bärwolff[1] and Michael Hinze[2]

[1] TU Berlin, Institute of Mathematics, D-10623 Berlin, Str. d. 17. Juni 135, Germany
[2] TU Dresden, Institute of Mathematics, D-01062 Dresden, Zellescher Weg 12-14, Germany

1 Introduction

During the growth of crystals in axisymmetric zone melting devices the transition from the twodimensional flow regime to an unsteady threedimensional behavior of the velocity and temperature field is observed in experiments under certain conditions of the growth device. This behavior leads to so called striations which from the crystal quality point of view should be avoided during the growth process. To avoid such crystal defects it is important to figure out those parameters, which guarantee a stable steady twodimensional melt flow during the growth process. There are several possibilities to determine these parameters. In the present work an optimization approach will be discussed.
From experiments and practical crystal production processes it is known that unsteady behavior of the melt and vorticies near the fluid-solid-interphase decrease the crystal quality. From the optimization point of view it therefore makes sense to gain

(i) flows, which are nearly steady, and/or
(ii) flows, which only have small vorticity in a certain region of the melt zone.

In a mathematical setting the goal in (i) may be achieved by minimizing tracking-type functionals of the form

$$J(\boldsymbol{u}, \theta_c) = \frac{1}{2} \int_0^T \int_\Omega |\boldsymbol{u} - \overline{\boldsymbol{u}}|^2 \, d\Omega dt + \frac{\alpha}{2} \int_0^T \int_{\Gamma_c} (\theta_c^2 + \theta_{c_t}^2) \, d\Omega dt, \qquad (1)$$

whereas goal (ii) may be related to minimal values of vorticity-type functionals of the form

$$J(\boldsymbol{u}, \theta_c) = \frac{1}{2} \int_0^T \int_\Omega |curl\boldsymbol{u}|^2 \, d\Omega dt + \frac{\alpha}{2} \int_0^T \int_{\Gamma_c} (\theta_c^2 + \theta_{c_t}^2) \, d\Omega dt \, . \qquad (2)$$

Above, $\boldsymbol{u}$ denotes the flow velocity vector field in the melt, and $\overline{\boldsymbol{u}}$ the desired state, which represents a physically favourable flow situation. The function θ_c denotes the temperature flux on the wall of the crucible and serves as control variable on the control boundary Γ_c. Both cost functionals contain two parts; the first part provides the mathematical formulation of the control gain, and the second part weighs the control cost.

2   Mathematical model

The flow in the crystal melt is gouverned by the Boussinesq approximation of the Navier-Stokes system for the velocity $\boldsymbol{u} = (u, v, w)$, the pressure p and the temperature θ;

$$
\left.
\begin{aligned}
\boldsymbol{u}_t + (\boldsymbol{u} \cdot \nabla)\boldsymbol{u} - \Delta\boldsymbol{u} + \nabla p - Gr\,\theta\,\boldsymbol{g} = 0 \quad \text{on } \Omega_T, \\
-\operatorname{div}\boldsymbol{u} = 0 \quad \text{on } \Omega_T, \\
\theta_t + \boldsymbol{u} \cdot \nabla\theta - \tfrac{1}{Pr}\Delta\theta - f = 0 \quad \text{on } \Omega_T.
\end{aligned}
\right\}
\tag{3}
$$

Here $\boldsymbol{g} = (0, 0, 1)$ and $\Omega_T = \Omega \times (0, T)$ denotes the space-time cylinder with cylindrical melt zone of height H and radius R. Furthermore, Gr denotes the Grashof number, and Pr the Prandtl number. Since in the present work we are mainly interested in control via boundary temperatures the absence of external forces is assumed.

System (3) is supplied with temperature boundary conditions of third kind on the crucible walls (which form the control boundary Γ_c), and at the solid-liquid interface Γ_d the melting temperature is prescribed, and Dirichlet boundary conditions at the remaining parts of the boundary. For the flow Dirichlet boundary conditions are prescribed on the whole boundary Γ. More precisely we set

$$
\left.
\begin{aligned}
u = u_d, \ v = v_d, \ w = w_d \quad \text{on } \Gamma_T, \\
\lambda\frac{\partial\theta}{\partial\mathbf{n}} + \tilde{a}(\theta - \theta_0) = \theta_c \quad \text{on } \Gamma_{cT}, \\
\theta = \theta_d \quad \text{on } \Gamma_{dT},
\end{aligned}
\right\}
\tag{4}
$$

where $\Gamma_T := \Gamma \times [0, T]$, θ_0 is some environmental temperature and $\lambda, \tilde{a}$ denote physical constants. From now onwards it is convenient to rewrite the boundary condition on Γ_c in the form

$$
a\frac{\partial\theta}{\partial\mathbf{n}} + b\theta = \theta_c \quad \text{on} \quad \Gamma_{cT},
\tag{5}
$$

with appropriate coefficients a, b which may not vanish simultaneously. We note that it is possible to include via u_d, v_d, w_d certain crystal and crucible rotations, as it is common in the case of Czochralski growth. In the case of zone melting techniques one would require $\boldsymbol{u} = \boldsymbol{0}$.

Finally let us discuss the initial values for (3). The initial velocity is chosen as the neutral position of the crystal melt, i.e.

$$
\boldsymbol{u} = \boldsymbol{0}.
\tag{6}
$$

The initial temperature field is chosen as solution of

$$
-\frac{1}{Pr}\Delta\theta = 0 \text{ in } \Omega, \ \theta = \theta_0 \text{ on } \Gamma_c, \text{ and } \theta = \theta_d \text{ on } \Gamma_d.
\tag{7}
$$

The material properties and the dimensionless parameters depend on the specific application and have to be defined appropriately.

We assume that prescribing heat fluxes on the walls of the crucible is possible, so that boundary conditions of third kind can be utilized as control mechanism. The optimization goal then consists in finding an optimal boundary heating strategy by adjusting the heat fluxes. Once this strategy is known, in a further step the methods developed in [6] may be applied to provide optimal heater locations by solving an appropriate inverse problem.

Let us note that the choice of $a \equiv 0, b \neq 0$ includes Neumann boundary control, and $a \neq 0, b \equiv 0$ Dirichlet boundary control. However, effects related to radiation are excluded.

3   Optimization

The optimization problem considered in the present work is given by

$$(\text{P}) \qquad \begin{cases} \min J(y, \theta_c) \\ \text{s.t.} (3) - (7). \end{cases} \tag{8}$$

To derive the first order necessary optimality conditions for this optimization problem we formally utilize the Lagrange technique. The related Lagrangian in the primitive setting is given by

$$L(\boldsymbol{u}, p, \theta, \theta_c, \boldsymbol{\mu}, \xi, \kappa, \chi) = J(\boldsymbol{u}, \theta_c) + \langle \boldsymbol{\mu}, \boldsymbol{u}_t + (\boldsymbol{u} \cdot \nabla)\boldsymbol{u} - \Delta \boldsymbol{u} + \nabla p - Gr\,\theta\,\boldsymbol{g} \rangle_{\Omega_T}$$

$$-\langle \xi, div\,\boldsymbol{u} \rangle_{\Omega_T} + \langle \kappa, \theta_t + \boldsymbol{u} \cdot \nabla \theta - \frac{1}{Pr}\Delta\theta - f \rangle_{\Omega_T} + \langle \chi, a\frac{\partial\theta}{\partial\mathbf{n}} + b\theta - \theta_c \rangle_{\Gamma_{cT}}, \tag{9}$$

where $\langle \cdot, \cdot \rangle_{\Gamma_{cT}}$ and $\langle \cdot, \cdot \rangle_{\Omega_T}$ denote appropriate duality pairings, and $\boldsymbol{\mu}$, ξ, κ and χ are Lagrange parameters. For example for $\boldsymbol{u}, p$ and θ sufficiently regular one has

$$< \boldsymbol{\mu}, \boldsymbol{u}_t + (\boldsymbol{u} \cdot \nabla)\boldsymbol{u} - \Delta \boldsymbol{u} + \nabla p - Gr\,\theta\,\boldsymbol{g} >_{\Omega_T} =$$

$$\int_{\Omega_T} [\boldsymbol{u}_t + (\boldsymbol{u} \cdot \nabla)\boldsymbol{u} - \Delta \boldsymbol{u} + \nabla p - Gr\,\theta\,\boldsymbol{g}] \cdot \boldsymbol{\mu}\,d\Omega\,dt.$$

A precise functional analytic setting, also containing the convergence analysis of the solution algorithms proposed in the subsequent sections will be given in a forthcoming paper, see also [1,13,10].

The necessary optimality conditions for (P) are now given by

$$\nabla L = 0.$$

Assembling these conditions for the cost functions of (1) and (2) leads to the state equations (3)-(7), together with the so called adjoint system

$$
\left.
\begin{aligned}
-\boldsymbol{\mu}_t - \Delta\boldsymbol{\mu} + (\nabla\boldsymbol{u})^t\boldsymbol{\mu} - (\boldsymbol{u}\cdot\nabla)\boldsymbol{\mu} + \nabla\xi = -\kappa\nabla\theta + \begin{cases} -(\boldsymbol{u} - \overline{\boldsymbol{u}}) \\ \text{curl curl}\,\boldsymbol{u} \end{cases} & \quad \text{in } \Omega_T, \\
-\text{div }\boldsymbol{\mu} = 0 & \quad \text{in } \Omega_T \\
\boldsymbol{\mu} = \boldsymbol{0} & \quad \text{on } \Gamma_T, \\
\boldsymbol{\mu}(T) = \boldsymbol{0} & \quad \text{in } \Omega, \\[2mm]
-\kappa_t - \tfrac{1}{Pr}\Delta\kappa - \boldsymbol{u}\cdot\nabla\kappa = Gr\,\boldsymbol{g}\cdot\boldsymbol{\mu} & \quad \text{in } \Omega_T, \\
\kappa = 0 & \quad \text{on } \Gamma_{dT}, \\
a\tfrac{\partial\kappa}{\partial\mathbf{n}} + b\kappa = 0 & \quad \text{on } \Gamma_{cT}, \\
\kappa(T) = 0 & \quad \text{in } \Omega, \\[2mm]
\chi = \begin{cases} -\tfrac{1}{bPr}\tfrac{\partial\kappa}{\partial\mathbf{n}} & \text{if } b \neq 0 \\ \tfrac{1}{aPr}\kappa & \text{if } b = 0 \end{cases} & \quad \text{on } \Gamma_{cT},
\end{aligned}
\right\}
\tag{10}
$$

and the optimality conditions

$$
\begin{aligned}
\alpha(-\theta_{c_{tt}} + \theta_c) &= \chi \quad \text{on } \Gamma_{cT} \\
\theta_c(0) &= \theta_0 \quad \text{on } \Gamma_c, \\
\theta_{c_t}(T) &= 0 \quad \text{on } \Gamma_c.
\end{aligned}
\tag{11}
$$

Here θ_0 denotes a temperature distribution on Γ_c at the beginning of the melting process.

Alltogether, the necessary optimality conditions for problem (P) form a boundary value problem for $\boldsymbol{u}, p, \theta, \boldsymbol{\mu}, \xi$, and θ_c w.r.t. space and time in the space-time domain Ω_T, which inherits a very special structure.

From now onwards we assume that system (3) together with (4), (6) and (7) for given θ_c admits a unique solution (this is satisfied under appropriate assumptions at least in the two-dimensional case, see [5], [8]). Then the cost functionals in (1),(2) may be rewritten in the form

$$
\hat{J}(\theta_c) = J(\boldsymbol{u}(\theta_c), \theta_c),
$$

where the gradient of $\hat{J}$ is determined by the optimality condition (11). More precisley, there holds

$$
\hat{J}'(\theta_c) = \alpha(\theta c_{tt} + \theta_c) - \chi.
\tag{12}
$$

To evaluate $\hat{J}'(\theta_c)$ for given θ_c amounts to solving (3)-(7) for $\boldsymbol{u}, \theta$, and then (10) for $\boldsymbol{\mu}, \theta$ and χ.

In numerical computations it is advantageous to substiute the time derivative of θ_c in the cost functionals (1),(2) by some auxilliary variable η,

$$
\theta_{c_t} = \eta \text{ on } \Gamma_{cT}.
\tag{13}
$$

This results in the optimality condition

$$
\theta_{c_t} = \frac{1}{\alpha}\zeta, \quad \theta_c(0) = \theta_0 \quad \text{on } \Gamma_{cT}
\tag{14}
$$

$$
-\zeta_t = -\alpha\theta_c + \chi, \quad \zeta(T) = 0 \quad \text{on } \Gamma_{cT},
\tag{15}
$$

instead of the two point boundary value problem (11).

Let us close this section with noting that the approach to boundary control presented in the present work is designed to compute temperature distributions at every single point of the control boundary, since it follows from (12) that the gradient of the cost functional w.r.t. θ_c can be expressed in terms of adjoint variables, so that the directional derivatives in all directions are available once the adjoint variables are determined. This is different to the approach presented in e.g. [9], were control functions are sought which only depend on a few numbers of parameters and directional derivatives w.r.t these parameters are computed using finite difference techniques. We note that the latter approach requires the solution of an auxilliary linear problem for every directional derivative, so that its computationally complexity is proportional to the number of parameters.

4   The numerical approach

We solve problem (8) by applying a damped Picard iteration to the KKT system (3)-(7), (10),(11). The pseudo-algorithm reads

  i) choose θ_c,
 ii) solve the forward problem for $[\boldsymbol{u}, \theta](\theta_c)$
iii) solve the adjoint problem for $[\boldsymbol{\mu}, \kappa](\boldsymbol{u}, \theta)$
 iv) update $\theta_c := \sigma_r \theta_c + (1 - \sigma_r)\mathcal{H}^{-1}(\chi)$, $\sigma_r \in]0, 1[$,
  v) until convergence, go to ii),

where $\mathcal{H}^{-1}(\chi)$ for given χ denotes the solution of (11).

Next let us describe the numerical solution methods used in ii)-iv). For this purpose we denote by $t_i := i\tau$, $i = 0, \ldots Z$ an equidistant time grid on $[0, T]$, where $\tau := \frac{T}{Z}$ for some $Z \in \mathbb{N}$. Moreover, unknown quantities are supplied with superscripts. In ii) we apply a semi-implicit time discretization scheme. Convective terms are treated explicitly, conductive terms implicitly. We obtain for $n = 0, \ldots, Z - 1$

$$\frac{\boldsymbol{u}^{n+1}}{\tau} - \Delta \boldsymbol{u}^{n+1} + \nabla p^{n+1} - Gr\, \theta^{n+1}\boldsymbol{g} = \frac{\boldsymbol{u}}{\tau} - (\boldsymbol{u} \cdot \nabla)\boldsymbol{u}, \tag{16}$$

$$-div\, \boldsymbol{u}^{n+1} = 0, \tag{17}$$

$$\frac{\theta^{n+1}}{\tau} - \frac{1}{Pr}\Delta\theta^{n+1} = \frac{\theta}{\tau} - (\boldsymbol{u} \cdot \nabla)\theta, \tag{18}$$

supplied with the boundary conditions (4) at $t = t_{n+1}$. Here $\boldsymbol{u}$ and θ for $n = 0$ are taken from (6) and (7), respectively. Of course, given $\boldsymbol{u}$ equation (18) can be solved for θ^{n+1}. To solve (16),(17) we apply a pressure-correction scheme which is explained next. Taking the divergence in (16) leads to

$$-\Delta p^{n+1} = -\frac{1}{\tau}div\, \hat{\boldsymbol{u}}, \tag{19}$$

where

$$\hat{\boldsymbol{u}} = \boldsymbol{u} + \tau[(\boldsymbol{u} \cdot \nabla)\boldsymbol{u} + Gr\, \theta^{n+1}\boldsymbol{g}]. \tag{20}$$

For the pressure we get Neumann boundary conditions. In the case of no slip walls the pressure boundary conditions are of the form $\frac{\partial p^{n+1}}{\partial \boldsymbol{n}} = 0$. Using the noted boundary conditions for p^{n+1} equation (19) can be solved for p^{n+1}, which in turn determines the velocity field $\boldsymbol{u}^{n+1}$ in terms of

$$\frac{1}{\tau}\boldsymbol{u}^{n+1} - \Delta\boldsymbol{u}^{n+1} = \frac{1}{\tau}\boldsymbol{u} - \nabla p^{n+1} \tag{21}$$

together with boundary conditions for $\boldsymbol{u}^{n+1}$ from (4) for $t = t_{n+1}$. In summary step ii) amounts to solving one poisson equation for p^{n+1}, three Helmholtz equations for $\boldsymbol{u}^{n+1}$, and one for θ^{n+1}. Spatially these subproblems are discretized by the finite volume method on a staggered grid in cylindrical coordinates developed in [2]. The resulting linear systems are solved by appropriately preconditioned cg methods.

For the time discretization of the adjoint system in iii) we for $n = Z, \ldots, 1$ apply the scheme

$$\frac{\boldsymbol{\mu}^{n-1} - \boldsymbol{\mu}}{\tau} - \Delta\boldsymbol{\mu}^{n-1} + (\nabla\boldsymbol{u}^{n-1})^t\boldsymbol{\mu} - (\boldsymbol{u}^{n-1} \cdot \nabla)\boldsymbol{\mu} + \nabla\xi^{n-1}$$
$$= -\kappa^{n-1}\nabla\theta + \begin{cases} -(\boldsymbol{u}^{n-1} - \overline{\boldsymbol{u}}) \\ \text{curl curl } \boldsymbol{u}^{n-1}, \end{cases} \tag{22}$$

$$-div\,\boldsymbol{\mu}^{n-1} = 0, \tag{23}$$

$$\frac{\kappa^{n-1} - \kappa}{\tau} - \boldsymbol{u}^{n-1} \cdot \nabla\kappa - \frac{1}{Pr}\Delta\kappa^{n-1} = Gr\,\boldsymbol{g} \cdot \boldsymbol{\mu}, \tag{24}$$

where for $n = Z$ we have $\boldsymbol{\mu} = \mu(T) = 0$ and also $\kappa = \kappa(T) = 0$. The boundary conditions are taken from (10) for $t = t_{n-1}$. A motivation of this scheme together with a detailed discussion is given in the appendix. Eq. (24) immediately can be solved for κ^{n-1}, the quantities $\boldsymbol{\mu}^{n-1}, \xi^{n-1}$ are obtained from (22),(23) by the pressure-correction method explained above. Spatially these subproblems are discretized again by the finite volume method of [2], and the resulting linear systems are also solved by appropriately preconditioned cg methods.

To provide $\mathcal{H}^{-1}(\chi)$ in iv) eq. (11) is solved for the control θ_c by a finite volume method in space and time, where the boundary conditions $\theta_c(\gamma, 0) = \theta_{c0}$ and $\theta_{c_t}(\gamma, T) = 0$ for $\gamma \in \Gamma_c$ are taken. We note that $\mathcal{H} := -\partial_{tt} + id$.

Let us note that for the computation of $\boldsymbol{\mu}^{n-1}, \xi^{n-1}, \kappa^{n-1}$ the flow $\boldsymbol{u}^{n-1}$ is required for $n = Z, \ldots, 1$. This means that we have to store these flow velocities in order to compute the adjoint solution $\boldsymbol{\mu}^{n-1}, \kappa^{n-1}$, and θ_c.

Let us close this section with describing the numerical approach that we take to tackle (13)-(15). With the notations from above it is given by

$$\frac{\theta_c^{n+1} - \theta_c^n}{\tau} = \frac{1}{\alpha}\zeta^{n+1}, \; n = 0, \ldots, Z-1, \; \theta^0 = \theta_0 , \tag{25}$$

$$-\frac{\zeta^{n+1} - \zeta^n}{\tau} = -\alpha\theta_c^n + \chi^n, \; n = Z-1, \ldots, 0, \; \zeta^Z = 0. \tag{26}$$

5   Results of the numerical solution of the full problem

First testproblem
As a first testproblem we consider a zone melting configuration with Dirichlet boundary control, i.e. we set $a \equiv 0, b := 1$. We use the crystal $(Bi_{0.25}Sb_{0.75})_2Te_2$, a composition of bismuth point fifty antimony one point fifty telurium two, whose geometrical and material parameters are summarized in Table 1 (see also [2]).

$(Bi_{0.25}Sb_{0.75})_2Te_2$-crystals are used for small cooling devices. The Fig. 1 shows the physical domain of the melt zone. For the velocity we have homogeneous
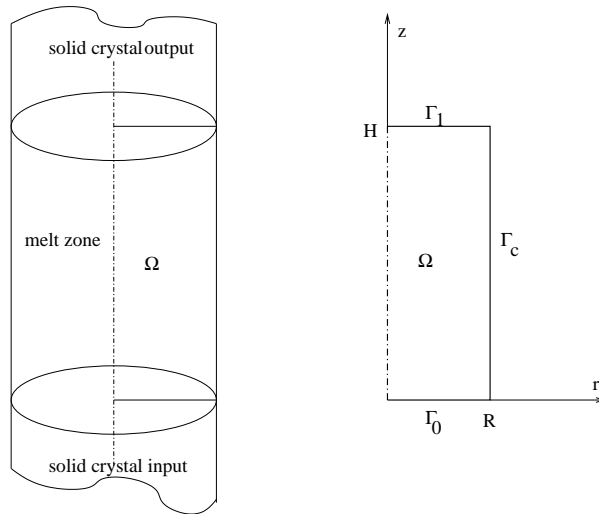
Fig. 1. Physical domain for the zone melting growth

Dirichlet data on the whole boundary. For the temperature we have the boundary

parameter	symbol	value
radius of the ampulla	R	$0.004\ m$
height of the melt	H	$0.016\ m$
melting point temperatur	θ_s	$613\ K$
thermal diffusivity	a	$0.44000\text{e-}05\ \frac{m^2}{s}$
kinematic viscosity	ν	$0.36310\text{e-}06\ \frac{m^2}{s}$
thermal expansion coefficient	β	$0.96000\text{e-}04\ K^{-1}$

Table 1. Parameters of $(Bi_{0.25}Sb_{0.75})_2Te_2$-melt and of the melt geometry

conditions

$$\theta = \theta_c \quad \text{for } r = R, 0 \le z \le H, \varphi \in (0, 2\pi), \text{ (control boundary } \Gamma_c) \quad (27)$$

$$\theta = \theta_s, \quad \text{for } 0 \le r \le R, z = H, \quad (28)$$

$$\theta = \theta_s, \quad \text{for } 0 \le r \le R, z = 0. \quad (29)$$

For $t = 0$ we start with a given temperature profile $\theta_c = \theta_{c0}$ on Γ_c, and with $\theta_s = 613\,K$. For θ_{c0} we have

$$\theta_{c0}(z) = \theta_s + 4\frac{z}{H}(1 - \frac{z}{H})\delta\theta \quad (30)$$

with $\delta\theta = 25\,K$. The control goal is tracking of a velocity field $\overline{\boldsymbol{u}}$, which either is given by

i) a typical twodimensional toroidal flow, or by a
ii) a non moving melt, i.e. $\overline{\boldsymbol{u}} = \boldsymbol{0}$.

The case ii) is artificial but serves as a good test case since $\theta_c = \theta_s = const.$ implies $\boldsymbol{u} = \boldsymbol{0}$, and this velocity field together with $\theta = \theta_s$ is a solution of the Boussinesq approximation. Artificial in this context means that $\theta = \theta_s$ on Ω is not a realistic assumption for a crystal melt and the input mixed crystal will never change to a single homogeneous output crystal. We consider the time interval $[0, T] = [0, 8\,\text{seconds}]$ and $Z = 60$ time steps of duration 0.1222 seconds each. For the given problems we use the optimization system (I). For the spatial discretization we use grid containing 20×30 finite volumes. As regularization and damping parameters we use $\alpha = 0.25$ and $\sigma_r = 0.1$. The Fig. 2 shows the results for case i), and Fig. 3 presents those of case ii). In both figures the left picture shows the development of the control temperature, whereas the right picture depicts the development of the functional value in relation to the iteration number of the Picard iteration. As can be seen the most significant reduction of the functional value already is achieved after the first few iterations. We note that the temperatures presented are dimensionless through the setting $\bar{\theta} = \frac{\theta - \theta_s}{\delta\theta}$.

Next we consider thermal boundary conditions second kind, i.e. $b \equiv 0$, so that

$$a\frac{\partial\theta}{\partial\mathbf{n}} = \theta_c \quad \text{for } r = R, 0 \le z \le H, \varphi \in (0, 2\pi), \text{ (control boundary } \Gamma_c), \quad (31)$$

and recall that for the adjoint temperature κ we have on Γ_c the boundary condition

$$\frac{\partial\kappa}{\partial\mathbf{n}} = 0 \quad \text{for } r = R, 0 \le z \le H, \varphi \in (0, 2\pi). \quad (32)$$

We start with $a = \lambda = 8,5\frac{W}{mK}$, $\theta_c = \theta_{c0} = 13000\frac{W}{m^2}$ and take the same geometrical and material parameters of the mixed crystal $(Bi_{0.25}Sb_{0.75})_2Te_2$ as above. The Fig. 4 shows the optimal $\bar{\theta}_c$ over the ampulla height and time (on
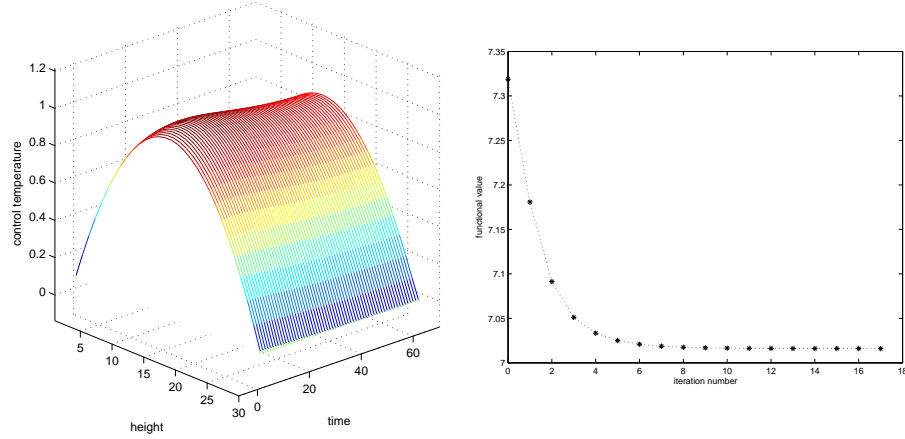
Fig. 2. Result of the zone melting process i)
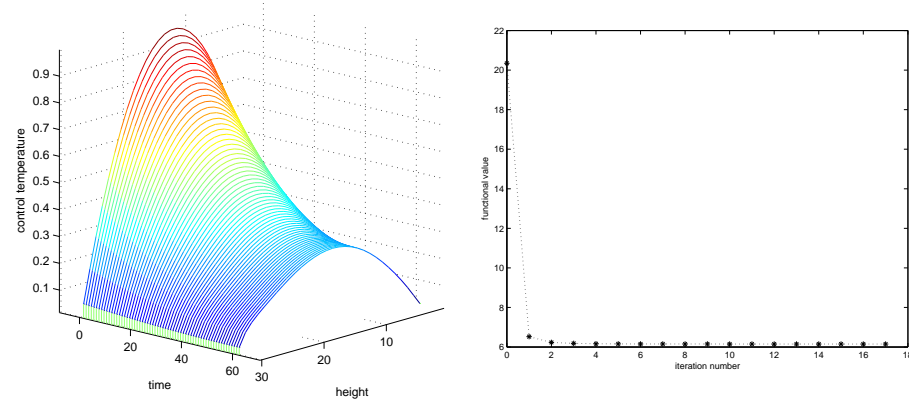
Fig. 3. Result of the zone melting process ii)

Γ_{cT}) and the development of the functional values vs. the iteration counter, where the dimensionless control temperature $\bar{\theta}_c$ now is defined as

$$\bar{\theta}_c = \frac{H\,\theta_c}{\delta\theta\,\lambda}\ .$$

If we set $\overline{\boldsymbol{u}} = \boldsymbol{0}$ we get the optimization results shown in Fig. 5. As you can see the optimal temperature distribution is nearly independent of time. This behaviour can be explained by the fact that a forward simulation with constant in time temperature $\theta_c(z,t) = \theta_{c0}(z)$, with θ_{c0} from (30) yields a velocity field $\boldsymbol{u}$ for which $\boldsymbol{u}(x,T)$ is very similar to $\overline{\boldsymbol{u}}(x)$.

Second testproblem
As a second testproblem we consider a (idealized) Czochralski crystal growth pro-
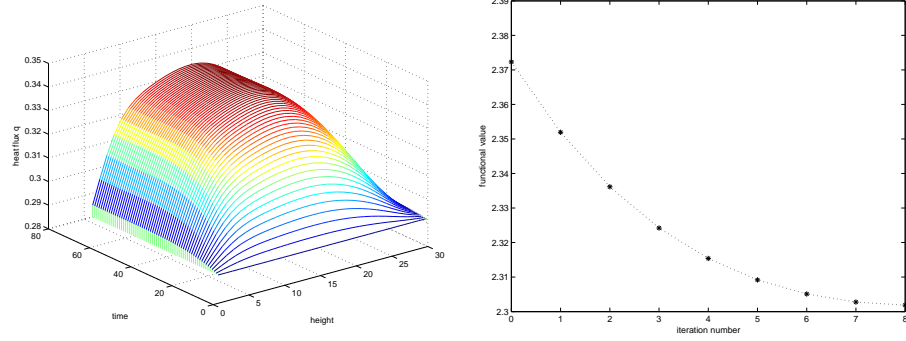
Fig. 4. Result of the optimization of the heating parameter $\bar{\theta}_c$
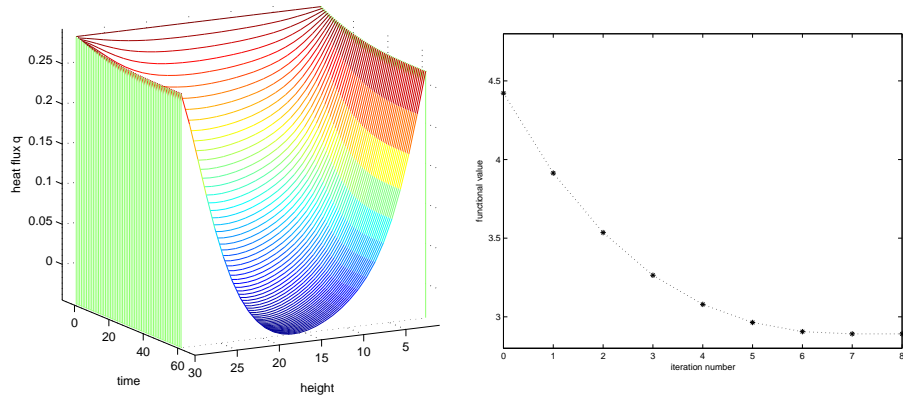
Fig. 5. Result of the optimization of the heating parameter $\bar{\theta}_c$

cess. The Fig. 6 shows the geometrical configuration of the crucible. The above discussed model and the optimization system is formulated and implemented in three dimensions. However, because of the huge computational amount of work in three spatial dimensions we first test the optimization procedure for the twodimensional case $u = 0$ (azimuthal component of the velocity) and $\frac{\partial Q}{\partial \varphi} = 0$ for all transport quantities Q ($\boldsymbol{u}, p, \theta$, etc.). Thus we consider a two-dimensional spatial domain (see Fig. 6). R_c is the radius of the solid crystal, R the crucible radius and H is the height of the crystal melt. θ_s denotes the melting point temperature of the crystal material, θ_b and θ_t are temperatures with $\theta_b > \theta_t > \theta_s$. The geometrical and material parameters are taken for the Silicium Czochralski growth process of [12] and are summarized in the Table 2.

The associated Grashof number is given by $1.5e + 09$ and leads to a strong CFL restriction for time stepping in our time discretization scheme. Time steps τ should not be taken larger than 10^{-5}. However, from the practical point of view this requirement is not as restrictive as it seems to be, since one dimensionless time step $\tau = 10^{-5}$ corresponds to 0.80645 seconds real time.
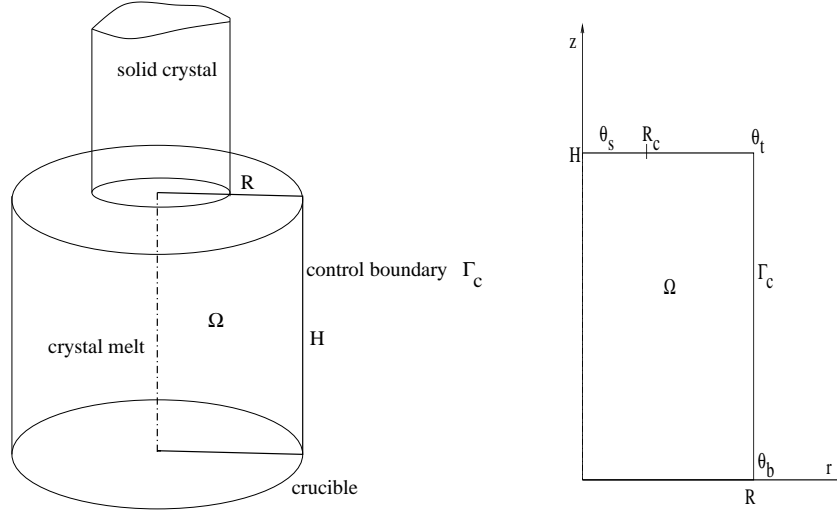
Fig. 6. Physical domain for Czochralski growth

Again we begin with investigating Dirichlet boundary control, i.e. we set $a \equiv 0$ and set $b := 1$. For the thermal boundary conditions of our Czochralski process we then have

$$\theta = \theta_c \quad \text{for } r = R, 0 \leq z \leq H, \varphi \in (0, 2\pi), \text{ (control boundary } \Gamma_c) \quad (33)$$

$$\theta = \theta_s, \quad \text{for } 0 \leq r \leq R_c, z = H, \quad (34)$$

$$\theta = \theta_s + \frac{r - R_c}{R - R_c}(\theta_t - \theta_s), \quad \text{for } R_c \leq r \leq R, z = H, \quad (35)$$

$$\theta = \theta_t, \quad \text{for } 0 \leq r \leq R, z = 0. \quad (36)$$

For $t = 0$ we start with a given temperature profile $\theta_c = \theta_{c0}$ on Γ_c and with $\theta_t = 1690\,K$, $\theta_b = 1708\,K$ for θ_{c0} we have

$$\theta_{c0}(z) = \theta_b + \frac{z}{H}(\theta_t - \theta_b) .$$

parameter	symbol	value
crucible radius	R	0.15 m
crystal radius	R_c	0.075 m
height of the melt	H	0.4 m
melting point temperature	θ_s	1683 K
thermal diffusivity	a	0.264e-04 $\frac{m^2}{s}$
kinematic viscosity	ν	0.279e-06 $\frac{m^2}{s}$
thermal expansion coefficient	β	$1.41*10^{-4}$ K^{-1}

Table 2. Parameters of Silicium and of the melt geometry
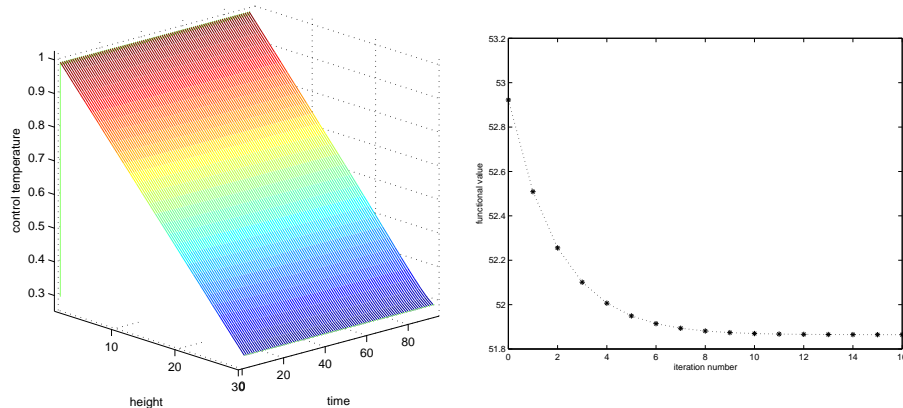
Fig. 7. Result of the optimization of the Czochralski process

As desired velocity field $\overline{\boldsymbol{u}}$ we use a typical toroidal steady twodimensional velocity field obtained from a forward Czochralski flow computation with the parameters of Table 2. The Fig. 7, left shows the temperature θ_c on Γ_{cT} for a time horizon containing 90 time steps (= 68,4 seconds). The right picture again shows the development of the functional value vs. the iteration counter. In this computations $\alpha = 0.5$ is taken as regularization parameter, and the relaxation parameter is chosen $\sigma_r = 0.75$. The temperatures $\bar{\theta}$ in the Fig. 7 are dimensionless i.e.

$$\bar{\theta} = \frac{\theta - \theta_b}{\theta_t - \theta_b} \ .$$

The control boundary temperatures do not alter significantly over the time horizon considered in the computation, see Fig. 7. This may be due to the similarity of the velocity field $\overline{\boldsymbol{u}}$ and the velocity field $\boldsymbol{u}$ at the time $t = T$. However, the develompent of the functional values vs. the iteration counter shows that the optimization works in principle. These results confirm the experiences of Gunzburger et al. in [9] who showed that boundary control is not very effective in the case of Czochralski growth.

Third testproblem

As a threedimensional testproblem we consider the zone melting configuration of Fig. 1. The aim of the optimization is to track the velocity field $\overline{\boldsymbol{u}} = \boldsymbol{0}$. For the spatial discretization of the domain $[0, 2\pi] \times [0, R] \times [0, H]$ we use a $20 \times 20 \times 30$ grid which is chosen equidistant in every coordinate direction. We consider the time interval $[0, T] = [0, 4\,\text{seconds}]$ with $Z = 60$ time steps of duration 0.0661 seconds each. The parameters $\alpha = 0.5$ and $\sigma_r = 0.1$ are used for the threedimensional testproblem. Fig. 8 shows the control temperature $\theta_c(\varphi, z, t)$ at the time $t = T$ on Γ_c together with the development of the functional values during the optimization iteration. Note, that the temperature profile in Fig. 8 (left) shows $\theta_c(\varphi, z, T)$ for varying φ and z. As you can see the profile is
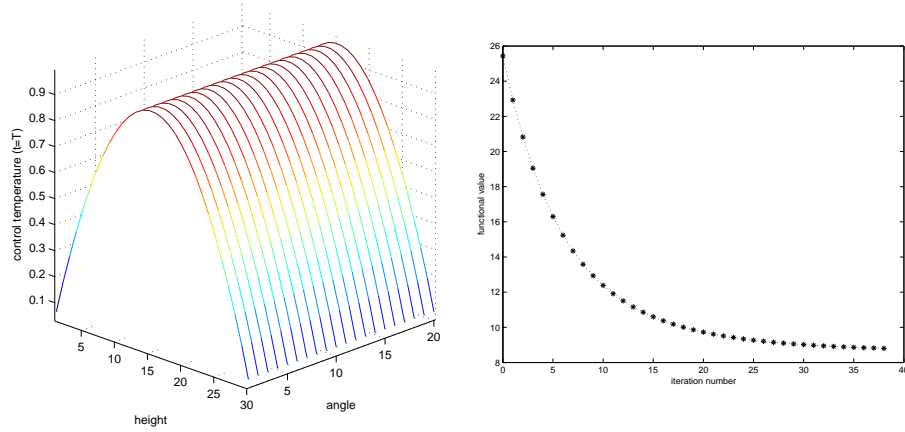
Fig. 8. Result of the optimization of the Czochralski process

nearly constant in circumferential direction. Of course, this behavior is expected since $\overline{\boldsymbol{u}} \equiv \boldsymbol{0}$. Furthermore, in view of the first testproblem, case ii), in the present testproblem one now would expect a behaviour of $\theta_c(0, z, t)$ similar to that shown in Fig. 3. And in fact is this the case, as Fig. 9 shows. Fig. 9 shows the control temperature $\theta_c(\varphi, z, t)$ on the line $\varphi = 0 = 2\pi$.

Compared to the second testproblem (Czochralski growth, $\sigma_r = 0.75 \ldots 0.90$) the consideration of the first and third testproblem show a significant sensibility of the Picard iteration procedure with regard to the damping parameter ($\sigma_r \leq 0.1$).

6   Conclusion

Optimal boundary heating control strategies for fully time-dependent thermally coupled flow problems in spatially 3-dimensional cylindrical domains are devel-
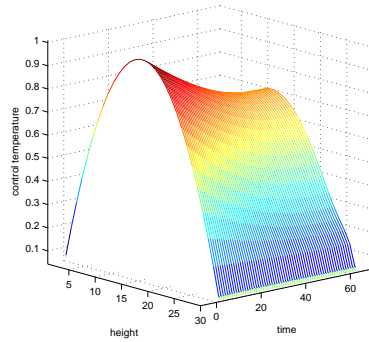
Fig. 9. control θ_c at $\varphi = 0$

oped. Optimal heating strategies are obtained as solutions of certain minimization problems and are computed from the related Karush-Kuhn-Tucker system by applying a damped Picard iteration.

Numerical results are presented for zone melting and Czochralski growth configurations in realistic 3-dimensional cylindrical domains. While boundary heating control for zone melting configurations seems to offer a practically relevant control mechanism the numerical results for Czochralski growth indicate, that boundary heating for this configuration seems to have only limited impact on the flow behaviour in the melt. As a result for Czochralski growth other control mechanisms should be considered, like control by magnetic fields and/or crucible/crystal rotation.

References

1. Abergel, F. and Temam, R. On some Control Problems in Fluid Mechanics. *Theoret. Comput. Fluid Dynamics*, 1:303–325, 1990.
2. Bärwolff, G., König, F. and G. Seifert: Thermal buoyancy convection in vertical zone melting configurations, ZAMM 77 (1997) 10
3. Hinze, M.: Optimal and instantaneous control of the instationary Navier-Stokes equations, habilitation thesis, Berlin, August 2000 (available on the webpage `http://www.math.tu-dresden.de/~hinze`)
4. Hinze, M.: Optimization of the Navier-Stokes equation, Adjoints workshop, Decin/Czech Republic, September 2001
5. Ladyzhenskaya, O.: The Mathematical Theory of Viscous Incompressible Flows, Gordon & Breach, 1969
6. Kurz, M.R.H.: Development of CrysVUN++, a Software System for Numerical Modelling and Control of Industrial Crystal Growth Processes, Thesis, Erlangen 1998
7. Kurz, M.R.H. and G. Müller : Control of thermal conditions during crystal growth by inverse modeling, Journal of Crystal Growth 208 (2000)
8. Constantin, P. and C. Foias: Navier-Stokes Equations, The University of Chicago Press, 1988
9. Gunzburger, M., Ozugurlu, E., Turner, J. and H. Zhang: Controlling transport phenomena in the Czochralski crystal growth process, Journal of Crystal Growth 234 (2002)
10. Hinze, M. and Kunisch, K. Second order methods for optimal control of time-dependent fluid flow. *SIAM J. Control Optim.*, 40:925–946, 2001.
11. Bärwolff, G.: Numerical Modelling of Two- and Three-Dimensional External and Internal Unsteady Incompressible Flow Problems, in: Computational Fluid Dynamics - Selected Topics, D. Leutloff and R.C. Srivastava (Eds.), Springer-Verlag Berlin Heidelberg New York, 1994
12. Böttcher, K.: Collected solid crystal and crystal melt material parameters, Berlin 2003 (available on the webpage `http://www.ikz-berlin.de/~kb`)
13. Temam, R. *Navier-Stokes Equations.* North-Holland, 1979.

7   Appendix

7.1   Derivatives of the governing equations

The directional derivatives of the Lagrangian (9) w.r.t. state and control variables are given by

$$L_{\boldsymbol{u}}\tilde{\boldsymbol{u}} = J_{\boldsymbol{u}}\tilde{\boldsymbol{u}} \tag{37}$$
$$+ <\boldsymbol{\mu}, mo_{\boldsymbol{u}} >_{\Omega_T} - <\xi, div\,\tilde{\boldsymbol{u}} >_{\Omega_T} + <\kappa, en_{\boldsymbol{u}} >_{\Omega_T} = 0,$$

$$L_p\tilde{p} = <\nabla\tilde{p}, \boldsymbol{\mu} >_{\Omega_T} = \int_{\Omega_T} \nabla\tilde{p}\cdot\boldsymbol{\mu}\,d\Omega\,dt = 0, \tag{38}$$

$$L_\theta\tilde{\theta} = <\boldsymbol{\mu}, mo_\theta >_{\Omega_T} + <\kappa, en_\theta >_{\Omega_T} + <\chi, a\frac{\partial\tilde{\theta}}{\partial\mathbf{n}} + b\tilde{\theta} >_{\Gamma_{cT}} = 0, \tag{39}$$

$$L_{\theta_c}\tilde{\theta}_c = J_{\theta_c}\tilde{\theta}_c + <-\chi, \tilde{\theta}_c >_{\Gamma_{cT}} = 0 , \tag{40}$$

where

$$J_{\boldsymbol{u}}\tilde{\boldsymbol{u}} = \int_{\Omega_T} (\boldsymbol{u} - \overline{\boldsymbol{u}})\cdot\tilde{\boldsymbol{u}}\,d\Omega dt , \tag{41}$$

$$J_{\theta_c}\tilde{\theta}_c = -\alpha\int_{\Gamma_{cT}} \theta_{c_{tt}}\tilde{\theta}_c d\Gamma_c\,dt + \int_{\Gamma_c} [\theta_{c_t}\tilde{\theta}_c]_0^T\,d\Gamma , \tag{42}$$

$$<\boldsymbol{\mu}, mo_{\boldsymbol{u}} >_{\Omega_T} = \int_{\Omega_T} [\tilde{\boldsymbol{u}}_t - \Delta\tilde{\boldsymbol{u}} + (\boldsymbol{u}\cdot\nabla)\tilde{\boldsymbol{u}} + (\tilde{\boldsymbol{u}}\cdot\nabla)\boldsymbol{u}]\cdot\boldsymbol{\mu}\,d\Omega dt, \tag{43}$$

$$<\boldsymbol{\mu}, mo_\theta >_{\Omega_T} = \int_{\Omega_T} -Gr\,\tilde{\theta}\boldsymbol{g}\cdot\boldsymbol{\mu}\,d\Omega dt , \tag{44}$$

$$<\kappa, en_{\boldsymbol{u}} >_{\Omega_T} = \int_{\Omega_T} [(\tilde{\boldsymbol{u}}\cdot\nabla)\theta]\kappa\,d\Omega dt , \tag{45}$$

$$<\kappa, en_\theta >_{\Omega_T} = \int_{\Omega_T} [\tilde{\theta}_t + \boldsymbol{u}\cdot\nabla\tilde{\theta} - \frac{1}{Pr}\Delta\tilde{\theta}]\kappa\,d\Omega dt. \tag{46}$$

Integration by parts combined with appropriate choices of test functions now straightforward lead to the equations (10), (11) for the adjoint variables $\boldsymbol{\mu}$, ξ, κ, χ, and the control variable θ_c. These variables together with the state equations (3)-(7) form the Karush-Kuhn-Tucker system. Details are left to the reader.

7.2   Construction of the adjoint time discretization

The time discretization of the adjoint system presented in (22)-(24) is based on the transpose of semi-impicit time discretization of the derivative of the Boussinesq approximation. To become more precise let us write (3) in the form

$$B(\boldsymbol{u}, p, \theta) = (0, f)^t.$$

Then the derivative of B in direction $\tilde{\boldsymbol{u}}, \tilde{p}, \tilde{\theta}$ is given by

$$B'(\boldsymbol{u}, p, \theta)(\tilde{\boldsymbol{u}}, \tilde{p}, \tilde{\theta}) = \begin{bmatrix} \tilde{\boldsymbol{u}}_t - \Delta\tilde{\boldsymbol{u}} + (\boldsymbol{u}\cdot\nabla)\tilde{\boldsymbol{u}} + (\tilde{\boldsymbol{u}}\cdot\nabla)\boldsymbol{u} + \nabla\tilde{p} - Gr\,\tilde{\theta}\boldsymbol{g} \\ -div\,\tilde{\boldsymbol{u}} \\ \tilde{\theta}_t + \boldsymbol{u}\cdot\nabla\tilde{\theta} + \tilde{\boldsymbol{u}}\cdot\nabla\theta - \frac{1}{Pr}\Delta\tilde{\theta} \end{bmatrix} . \tag{47}$$

The time discretization of (47) is adapted to that of the Boussinesq Approximation presented in (16)-(18). Again we denote by $t_i = i\tau$, $\tau = \frac{T}{Z}$ for some $Z \in \mathbb{N}$ an equidistant time grid. For $0 \leq n < Z$ we now set

$$D_\tau B'(\boldsymbol{u}, p, \theta)(\tilde{\boldsymbol{u}}^{n+1}, \tilde{p}^{n+1}, \tilde{\theta}^{n+1}) =$$
$$\begin{bmatrix} \frac{\tilde{\boldsymbol{u}}^{n+1} - \tilde{\boldsymbol{u}}}{\tau} - \Delta\tilde{\boldsymbol{u}}^{n+1} + (\boldsymbol{u} \cdot \nabla)\tilde{\boldsymbol{u}} + (\tilde{\boldsymbol{u}} \cdot \nabla)\boldsymbol{u} + \nabla\tilde{p}^{n+1} - Gr\,\tilde{\theta}^{n+1}\boldsymbol{g}, \boldsymbol{\mu} > \\ -div\,\tilde{\boldsymbol{u}}^{n+1} \\ \frac{\tilde{\theta}^{n+1} - \tilde{\theta}}{\tau} + \boldsymbol{u} \cdot \nabla\tilde{\theta} + \tilde{\boldsymbol{u}} \cdot \nabla\theta - \frac{1}{Pr}\Delta\tilde{\theta}^{n+1} \end{bmatrix}, \quad (48)$$

and note that all function values that appear without the superscript $n + 1$ are taken at time instance $t = t_n$. Next we set

$$\mathcal{A} = \frac{1}{\tau}id - \Delta, \quad \mathcal{B}_n = \frac{1}{\tau}id - (\boldsymbol{u} \cdot \nabla)(\,\cdot\,) - ((\,\cdot\,) \cdot \nabla)\boldsymbol{u}, \quad \mathcal{G} = \nabla, \quad \mathcal{F} = -Gr\,\boldsymbol{g},$$

$$\mathcal{D} = -div, \quad \mathcal{K} = (\,\cdot\,) \cdot \nabla\theta, \quad \mathcal{E} = \frac{1}{\tau}id - \frac{1}{Pr}\Delta, \mathcal{G} = \frac{1}{\tau}id - \boldsymbol{u} \cdot \nabla,$$

and introduce the block operators

$$A = \begin{pmatrix} \mathcal{A} & \mathcal{G} & \mathcal{F} \\ \mathcal{D} & 0 & 0 \\ 0 & 0 & \mathcal{E} \end{pmatrix} \quad \text{and} \quad B_n = \begin{pmatrix} \mathcal{B}_n & 0 & 0 \\ 0 & 0 & 0 \\ \mathcal{K} & 0 & \mathcal{G} \end{pmatrix}. \quad (49)$$

Further we set

$$\mathbf{x}^{n+1} = \begin{pmatrix} \tilde{\boldsymbol{u}}^{n+1} \\ \tilde{p}^{n+1} \\ \tilde{\theta}^{n+1} \end{pmatrix}, \quad \mathbf{x}^n = \begin{pmatrix} \tilde{\boldsymbol{u}} \\ \tilde{p} \\ \tilde{\theta} \end{pmatrix}$$

and note that

$$A\mathbf{x}^0 = \begin{pmatrix} \frac{\boldsymbol{u}_0}{\tau} - \Delta\boldsymbol{u}_0 + \nabla p_0 - Gr\,\boldsymbol{g}\theta_0 \\ 0 \\ \frac{\theta_0}{\tau} - \Delta\theta_0 \end{pmatrix}.$$

We are now prepared to rewrite the time discretization scheme (48) as

$$\mathcal{M}\mathbf{X} := \begin{pmatrix} A & \mathbf{0} \\ -B_0 & A & \mathbf{0} \\ \mathbf{0} & -B_1 & A \\ \cdots \\ & & & -B_{Z-2} & A & \mathbf{0} \\ & & & \mathbf{0} & -B_{Z-1} & A \end{pmatrix} \begin{pmatrix} \mathbf{x}^0 \\ \mathbf{x}^1 \\ \mathbf{x}^2 \\ \vdots \\ \mathbf{x}^{Z-1} \\ \mathbf{x}^Z \end{pmatrix}. \quad (50)$$

The tanspose of $\mathcal{M}$ now defines the discretization scheme (22)-(24) of the adjoint system (10). More precisely, let

$$\mathbf{y}^{n+1} = \begin{pmatrix} \boldsymbol{\mu}^{n+1} \\ \xi^{n+1} \\ \kappa^{n+1} \end{pmatrix} \quad \text{and} \quad \mathbf{y}^n = \begin{pmatrix} \boldsymbol{\mu} \\ \xi \\ \kappa \end{pmatrix} = \begin{pmatrix} \boldsymbol{\mu}^n \\ \xi^n \\ \kappa^n \end{pmatrix},$$

where $\boldsymbol{\mu}$, ξ and κ denote the adjoint variables, and set $\mathbf{Y} = (\mathbf{y}^0, \mathbf{y}^1, \ldots \mathbf{y}^Z)^t$. Then the time discretization scheme for the adjoint system is defined through

$$(\mathcal{M}\mathbf{X}, \mathbf{Y}) = (\mathbf{X}, \mathcal{M}^t\mathbf{Y}),$$

where

$$\mathcal{M}^t\mathbf{Y} = \begin{pmatrix} A^t & -B_0{}^t & \mathbf{0} & & & \\ \mathbf{0} & A^t & -B_1{}^t & \mathbf{0} & & \\ \cdots & & & & & \\ & & & A^t & -B_{Z-2}{}^t & \mathbf{0} \\ & & & \mathbf{0} & A^t & -B_{Z-1}{}^t \\ & & & & \mathbf{0} & A^t \end{pmatrix} \begin{pmatrix} \mathbf{y}^0 \\ \mathbf{y}^1 \\ \mathbf{y}^2 \\ \vdots \\ \mathbf{y}^{Z-1} \\ \mathbf{y}^Z \end{pmatrix}. \tag{51}$$

Applying this time-discretization procedure to (10) we obtain for $n = Z, Z - 1, \ldots, 1$

$$\frac{\boldsymbol{\mu}^{n-1} - \boldsymbol{\mu}}{\tau} + (\nabla \boldsymbol{u}^{n-1})^t \boldsymbol{\mu} - (\boldsymbol{u}^{n-1} \cdot \nabla)\boldsymbol{\mu} - \Delta \boldsymbol{\mu}^{n-1} + \nabla \xi^{n-1} \tag{52}$$

$$= -\kappa^{n-1} \nabla \theta + \begin{cases} -(\boldsymbol{u}^{n-1} - \overline{\boldsymbol{u}}) \\ \text{curl curl } \boldsymbol{u}^{n+1}, \end{cases}$$

$$-div\boldsymbol{\mu}^{n-1} = 0, \tag{53}$$

$$\frac{\kappa^{n-1} - \kappa}{\tau} + \boldsymbol{u}^{n-1} \cdot \nabla \kappa - \frac{1}{Pr} \Delta \kappa^{n-1} - Gr \, \boldsymbol{g} \cdot \boldsymbol{\mu}^{n-1} = 0 \tag{54}$$

which exactly represents (22)-(24).

7.3   Cylindrical coordinates

Since in our applications the Czochralski crucible and the zone melting ampulla have cylindrical geometry it is convenient to present the Boussinesq approximation in cylindrical coordinates. W.r.t. these coordinates it has the form

$$u_t + (ruu)_r/r + (uv)_\varphi/r + (wu)_z - v^2/r = \tag{55}$$
$$- p_r + ((ru)_r/r)_r + u_{\varphi\varphi}/r^2 + 2v_\varphi/r^2 + u_{zz} \,,$$

$$v_t + (ruv)_r/r + (vv)_\varphi/r + (wv)_z + uv/r = \tag{56}$$
$$- p_\varphi/r + ((rv)_r/r)_r + v_{\varphi\varphi}/r^2 - 2u_\varphi/r^2 + v_{zz} \,,$$

$$w_t + (ruw)_r/r + (vw)_\varphi/r + (ww)_z = \tag{57}$$
$$- p_z + (rw_r)_r/r + w_{\varphi\varphi}/r^2 + w_{zz} + Gr\,\theta \,,$$

$$(ru)_r/r + v_\varphi/r + w_z = 0 \,, \tag{58}$$

$$\theta_t + (ru\theta)_r/r + (v\theta)_\varphi/r + (w\theta)_z = \frac{1}{Pr}[(r\theta_r)_r/r + (\theta_\varphi)_\varphi/r^2 + (\theta_z)_z] \,. \tag{59}$$

To derive the adjoint system in cylindrical coordinates we set $\boldsymbol{\mu} = (\mu, \nu, \omega)$ where μ denotes the radial component, the azimutal component is ν, and the

z-component is ω. We now transfer the adjoint equations (10) to cylindrical coordinates an we get

$$-\mu_t - ((r\mu)_r/r)_r - \mu_{\varphi\varphi}/r^2 - 2\nu_\varphi/r^2 - \mu_{zz} + \mu(ru)_r/r + \nu v_r \qquad (60)$$
$$+\omega w_r - (u\mu)_r - (v\mu)_\varphi/r - (w\mu)_z + v\nu/r + \xi_r = -(u - \overline{u}) - \kappa\theta_r$$
$$-\nu_t - ((r\nu)_r/r)_r - \nu_{\varphi\varphi}/r^2 + 2\mu_\varphi/r^2 - \nu_{zz} \qquad (61)$$
$$+\mu u_\varphi/r + \nu v_\varphi/r + \omega w_\varphi/r + (\nu u - 2\mu v)/r$$
$$-(ru\nu)_r/r + (v\nu)_\varphi/r - (w\nu)_z + \xi_\varphi/r = -(v - \overline{v}) - \kappa\theta_\varphi/r$$
$$-\omega_t - (r\omega_r)_r/r - \omega_{\varphi\varphi}/r^2 - \omega_{zz} + \mu u_z + \nu v_z + \omega w_z \qquad (62)$$
$$-(ru\omega)_r/r - (v\omega)_\varphi/r - (w\omega)_z + \xi_z = -(w - \overline{w}) - \kappa\theta_z \ .$$

For the adjoint temperature κ we get

$$-\kappa_t - \frac{1}{Pr}[(r\kappa_r)_r/r + \kappa_{\varphi\varphi}/r^2 + \kappa_{zz}] - (ru\kappa)_r/r - (v\kappa)_\varphi/r - (w\kappa)_z = Gr\,\omega, \ \ (63)$$

which is a convective heat conduction equation whose discretization can be performed as in [2], say. We note that one also would obtain (60)-(63) as the adjoint part of the optimality system, if in the definition of the Lagrangian in (9) cylindrical coordinates for the constitutive equations would be used, together with the volume element $dV = dx\,dy\,dz$ of the integrals replaced by $r\,dr\,d\varphi\,dz$.

Having in mind the spatial discretization of the Navier-Stokes system on a staggered grid the terms

$$(\nabla\boldsymbol{u})^t\boldsymbol{\mu} \qquad \text{and} \qquad \kappa\nabla\theta$$

occuring in (60)-(62) are not standard terms. Using a staggered grid finite volume method, u and μ live at the same gridpoints, as do v and ν, w and ω, and θ and κ. Exemplarily we describe the discretization of the first component of both, $(\nabla\boldsymbol{u})^t\boldsymbol{\mu}$ and $\kappa\nabla\theta$. We obtain

$$(\mu u_r + \nu v_r + \omega w_r)_{i+1/2jk} \approx \qquad (64)$$
$$\mu_{i+1/2jk}[(u_{i+3/2jk} + u_{i+1/2jk}) - (u_{i+1/2jk} + u_{i-1/2jk})]/(2\Delta x_{i+1/2})$$
$$+\nu_{i+1/2jk}[(v_{i+1j+1/2k} + v_{i+1j-1/2k}) - (v_{ij+1/2k} + v_{ij-1/2k})]/(2\Delta x_{i+1/2})$$
$$+\omega_{i+1/2jk}[(w_{i+1jk+1/2} + w_{i+1jk-1/2}) - (w_{ijk+1/2} + w_{ijk-1/2})]/(2\Delta x_{i+1/2})$$

where

$$\nu_{i+1/2jk} = (\nu_{ij+1/2k} + \nu_{i+1j+1/2k} + \nu_{ij-1/2k} + \nu_{i+1j-1/2k})/4 \quad \text{and}$$

$$\omega_{i+1/2jk} = (\omega_{i+1jk+1/2} + \omega_{i+1jk-1/2} + \omega_{ijk+1/2} + \omega_{ijk-1/2})/4,$$

and

$$\kappa\theta_r \approx 0.5(\kappa_{i+1jk} + \kappa_{ijk})[\theta_{i+1jk} - \theta_{ijk}]/\Delta x_{i+1/2}. \qquad (65)$$